Geophys. J. Int. (1996) **126,** F7–F12

FAST-TRACK PAPER

410 km discontinuity sharpness and the form of the olivine α–β phase diagram: resolution of apparent seismic contradictions

George R. Helffrich and Bernard J. Wood

Geology Department, University of Bristol, Wills Memorial Building, Queens Road, Bristol BS8 1RJ, *UK*

Accepted 1996 June 17. Received 1996 June 12; in original form 1996 March 27

SUMMARY

Estimates of the thickness of the 410 km seismic discontinuity, believed to be due to the α-olivine$\rightarrow\beta$-modified-spinel transformation in olivine, are as low as 4 km based on discontinuity reflectivity. The seismically estimated thickness is, however, biased to values narrower than the true transformation interval if linear interpolation of properties is used for modelling. A 5 km linear velocity gradient yields an average reflection coefficient identical to that of a 10 km transition interval based on olivine phase-diagram features. Moreover, alternative forms of the phase diagram, equally consistent with experimentally determined iron–magnesium partitioning, can yield true transition intervals as narrow as 4 km. This reconciles a discrepancy between phase equilibrium and seismic measures of discontinuity thickness in two ways: (1) seismic thickness estimates are too narrow; and (2) narrow transition intervals are permissible given existing phase-equilibrium constraints. Incorporating recent results on the influence of H_2O on discontinuity properties, it appears that 410 km discontinuity reflectivity is much more sensitive to varying H_2O concentration than to temperature, suggesting that discontinuity reflectivity variations reflect changes in mantle chemistry.

Key words: mantle discontinuities, phase transitions, seismology.

1 INTRODUCTION

Upper-mantle periodotite consists of about 70 per cent olivine α-$(Mg,Fe)_2SiO_4$ with smaller amounts of pyroxene and garnet phases, in which the molar iron concentration (Fe/Fe + Mg) is about 0.1. At a pressure of approximately 14 GPa, corresponding in depth to the 410 km seismic discontinuity, the major α-phase is observed to transform to β-$(Mg,Fe)_2SiO_4$ (Fig. 1), with an increase in density of approximately 5.5 per cent. The demonstration of Revenaugh & Jordan (1991) that the depths of the Earth's major seismic discontinuities, at 410 and 660 km, are anticorrelated strongly supports the hypothesis that they are due to phase changes in mantle minerals (Bernal 1936; Ringwood 1969). Multivariant mineral reactions such as the α-olivine$\rightarrow\beta$-modified-spinel transformation ($\alpha\rightarrow\beta$) are, however, gradual rather than discontinuous, with the two phases coexisting over a finite depth interval. This feature is difficult to reconcile with seismic observations indicating an abrupt change in elastic properties with depth. Reported discontinuity thicknesses are in some cases 4 km or less (Benz & Vidale 1993; Yamazaki & Hirahara 1994; Neele 1996) based on the size of the reflection coefficient computed for linear velocity gradients. This is much narrower than the accepted $\alpha\rightarrow\beta$ transformation interval of 11–19 km (Katsura & Ito 1989; Akaogi, Ito & Navrotsky 1989), which suggests that some reassessment is warranted. The focus of this paper is to examine two possible explanations for the discrepant transformation interval sizes. The first is that the accepted phase-equilibrium transformation interval is too large and the second is that seismic results underestimate interval thickness. By exploring plausible limits on the phase-transformation interval obtained from high-pressure (Fe,Mg) partitioning between the α and β phases, we find that in the absence of H_2O and other trace components a range of transition thicknesses from 4 to 12 km is possible. This is clearly consistent with the seismic data. Furthermore, 0.5–1 Hz seismic-wave reflection coefficients are higher for realistic transition profiles than they are for the linear gradients with which they are typically approximated. Thus, thicker transition intervals may be compatible with short-period seismic observations because their equivalent reflectivity approaches that of thinner linear gradients. Finally, by comparing transition-interval broadening due to lateral variations in temperature with that due to bulk composition, we find that broadening is more sensitive to H_2O content than to temperature. The most likely cause of the observed variability in thickness of the 410 discontinuity is, therefore, bulk compositional fluctuations.

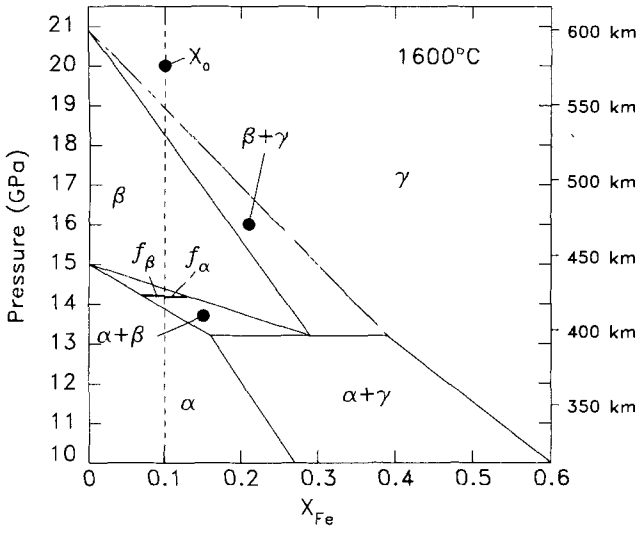

Figure 1. 1600 °C isothermal phase diagram in the $(Mg,Fe)_2SiO_4$ system after Katsura & Ito (1989). Single-phase regions are those marked α, β and γ and two-phase regions are identified with $\alpha+\beta$, $\alpha+\gamma$ and $\beta+\gamma$. Fe concentration in mantle olivines shown by the dashed line. Where this intersects the two-phase loops determines the pressure interval of two-phase coexistence. Relative lengths of line segments marked f_α and f_β to $\alpha+\beta$ field width denote proportions of α and β phases at a position in the transition interval.

2 PHASE-DIAGRAM PROPERTIES

Conservation of mass in a system of fixed bulk composition results in the so-called 'lever rule' where the molar proportions of the coexisting phases f_α and f_β are given by the relative lengths of the tie-lines lying to either side of the system bulk composition X_0 (Fig. 1). Approximating the boundaries $P_\alpha(X)$ and $P_\beta(X)$ of the two-phase region on a pressure–composition (P–X) phase diagram with straight lines that share a common intercept P_0 at X=0 and slopes b_α and b_β respectively,

$$f_\alpha = \begin{cases} k_1 - k_2\dfrac{1}{P-P_0}, & X_0 b_\alpha \le P - P_0 \le X_0 b_\beta, \\ 0, & P - P_0 > X_0 B_\beta, \\ 1, & P - P_0 < X_0 b_\alpha, \end{cases} \qquad (1)$$

revealing a fundamental $1/P$ dependence of phase proportion on pressure. The constants $k_1 = b_\alpha/(b_\alpha - b_\beta)$ and $k_2 = b_\alpha b_\beta X_0/(b_\alpha - b_\beta)$ describe the width and slope of the $\alpha \rightarrow \beta$ transition profile. Since the proportion of phases through a transition interval is not linear, as seismic modelling typically assumes (Richards 1972; Lees, Bukowinski & Jeanloz 1983; Benz & Vidale, 1993; Vidale, Ding & Grand 1995), it is, as shown below, likely that seismic reflectivity is underestimated for a phase transition such as $\alpha \rightarrow \beta$.

3 THE OLIVINE PHASE DIAGRAM

3.1 Shape effect

The boundaries of the two-phase region are generally curves rather than the straight lines assumed above, tending to enhance non-linearities in the elastic property profiles through the transition interval (Meijering & Rooymans 1958). To demonstrate the importance of curvature on reflectivity, we show schematic phase diagrams of fixed, 10 km transition widths with different curvatures broadly consistent with the experimental Fe–Mg partitioning data obtained at 1600 °C by Katsura & Ito (1989). P–X diagrams and their phase proportions through the transition interval are shown in Fig. 2. From these phase diagrams we compute short-period reflectivity profiles using a Haskell propagator methodology (Aki & Richards 1980). The velocities and densities used in these calculations are proportional combinations of properties from the IASP91 earth model (Kennett & Engdahl 1991) based on f_α for each profile. Olivine α properties are approximated by the IASP91 values above the discontinuity at 410 km and β-modified-spinel below it, extrapolated in depth as necessary using the gradients above and below the discontinuity. This approximation is justified because the elastic properties of the inert [non-$(Mg,Fe)_2SiO_4$] mineral components in the mantle increase roughly linearly through the 10 km intervals of interest. Fig. 3 shows underside P reflectivity profiles for the phase diagrams as a function of frequency from 0 to 2 Hz and averaged over 0.5 to 1 Hz. Though the transition intervals are equally thick, their reflectivities differ. Between 0.5 and 1 Hz, the reflectivity derived from the more strongly curved phase boundary with a 10 km transition interval approximates that of a 5 km linear profile. It is clear, therefore, that comparison of transition reflectivities with linear profiles generally underestimates transition interval thicknesses.

3.2 Feasible alternative forms

Whether the α–β transition interval is indeed 10 km, or whether a strong curvature for the phase diagram is thermochemically plausible, may be assessed by examining the solid-solution properties of olivine α and β-modified-spinel, which control the shape of the two-phase loop. Our goal here is not to present a definitive $\alpha+\beta$ thermodynamic model, but to show that alternative forms are feasible given phase-equilibrium constraints. Both solid solutions may be modelled as binary subregular solutions (Thompson 1967) where the excess free energy of solution $G^{xs} = W_{FeMg}X_{Fe}X_{Mg}^2 + W_{MgFe}X_{Mg}X_{Fe}^2$, but recent data suggest olivine solutions are essentially regular (Wiser & Wood 1991), with $W_{FeMg} = W_{MgFe} = W$. Adopting an interaction parameter W of 1770 cal (Wiser & Wood 1991) and the end-member solid-solution properties listed in Table 1, we explored about 1000 different subregular interaction-parameter combinations by grid search in the range $\pm$30 kcal in 1 kcal increments and computed phase diagrams to determine both two-phase loop shape and transition-interval thicknesses. We also explored models that incorporate the internal (Fe,Mg) ordering in β found in a single-crystal structure refinement of β-$(Mg_{0.9}Fe_{0.1})_2SiO_4$ synthesized at high pressure and temperature (Sawamoto & Horiuchi 1990). Only those diagrams compatible with (Fe,Mg) partitioning data (Katsura & Ito 1989; BJW unpublished data 1996) were considered to be acceptable. Element partitioning data provide the best constraint on the shape of the two-phase loop principally because they are only weakly sensitive to pressure and thus largely independent of experimental pressure uncertainties, which may be 5–10 per cent in multi-anvil apparatus. The end-member properties we used (Table 1) are within the uncertainties of the experimentally constrained 1 bar enthalpies and entropies reported by Akaogi *et al.* (1989). The diagrams

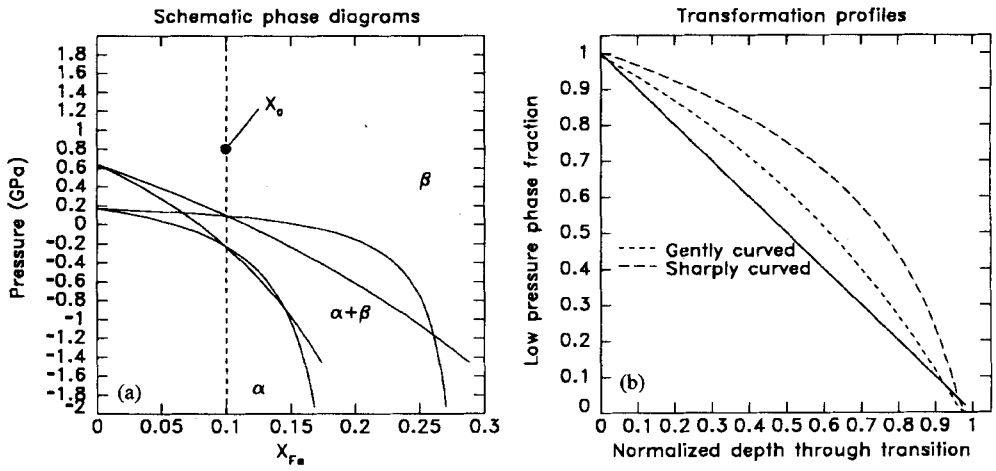

Figure 2. (a) Schematic phase diagrams consistent with experimentally determined (Fe,Mg) partitioning between α and β (Katsura & Ito 1989) having equivalent transition interval thicknesses, 0.3 GPa (10 km). The pressure scale is relative because the diagrams are shifted to emphasize their identical transition intervals for mantle composition X_0 (Jeanloz & Thompson 1983) (dashed line). (b) Molar proportions of coexisting α and β phases through the transition intervals for the two profiles in (a) compared to a linear gradient. For the sharply curved phase boundaries, half of the transition occurs in the final 25 per cent of the depth interval.

Table 1. End-member thermochemical data.

	V_{298K} cm^3 mol^{-1}	H^0_{1000K} kcal mol^{-1}	S^0_{1000K} cal K^{-1} mol^{-1}	$C_{P,1000K}$ cal K^{-1} mol^{-1}	γ_{th}	α K^{-1}×10^5	K_s Mbar	δ_s	dK_s/dP
α Mg_2SiO_4	43.67	-15.140	66.23	41.58	1.20	3.997	1.29	4.0	5.2
α Fe_2SiO_4	46.27	-6.560	83.47	46.18	1.10	3.700	1.38	5.5	5.2
β Mg_2SiO_4	40.52	-8.587	64.45	40.78	1.30	3.572	1.74	4.3	4.8
β Fe_2SiO_4	43.22	-3.161	81.43	46.06	1.30	3.200	1.89	5.6	4.8

Source: Bina & Wood (1987), with β-Mg_2SiO_4 H^0_{1000K} and S^0_{1000K} adjusted to yield α→β Mg_2SiO_4 transition pressures reported by Katsura & Ito (1989). Olivine regular solution $W = 1770$ cal $+ 0.006\,P$ cal bar^{-1} for mixing on two sites. β non-convergent ordering model recognizes 1 M1, 1 M2 and 2 M3 sites in the phase (Sawamoto & Horiuchi 1990) with equivalent mixing properties on the M1 and M3 sites. Internal regular solution mixing W_{M1} and W_{M2} are 1500 cal, −6200 cal for mixing on two sites and ΔG of the ordered and anti-ordered phases $Mg_{1.5}Fe_{0.5}SiO_4$ and $Fe_{1.5}$ $Mg_{0.5}$ SiO_4 are 700 and 3300 cal higher than a mechanical mixture of the Mg_2SiO_4 and Fe_2SiO_4 end-members, respectively.

consistent with (Fe,Mg) partitioning data encompass transition intervals ranging from 4 to 12 km thick (0.15 to 0.4 GPa in pressure). Three typical diagrams with transition intervals between 4 and 7 km are shown in Fig. 4. Their transition intervals are centred above the 13.6 GPa pressure at 410 km depth but are within the joint experimental- and pressure-scale uncertainties and thus are plausible models for the 410 seismic discontinuity. We find that by modelling β-modified-spinel as a subregular (Fe,Mg) solution, thin, 5–6 km transition intervals are feasible, but transitions more curved than those shown in Fig. 4 are not. Taking explicit account of Mg preference for the M2 site in β-$(Mg,Fe)_2SiO_4$ yields transition intervals as narrow as 4 km (Fig. 4). The principal reason that our results differ from those of Katsura & Ito (1989) and Akaogi *et al* (1989) is that we take explicit account of pressure uncertainty in multi-anvil apparatus, allowing the composition brackets to shift in pressure (due to P uncertainty), which permits compatibility with narrower phase loops.

3.3 Effect of H_2O and temperature

Both temperature and bulk compositional differences affect the form of the two-phase α+β region in the olivine phase diagram. Wood (1995) showed how water, a minor mantle constituent incorporated into the structure of nominally anhydrous minerals, influences the properties of the α–β transition. Because H_2O strongly prefers the β phase to α, the presence of H_2O stabilizes β over a wider range of pressures and temperatures, broadening the transition interval. Fig. 5 shows calculated 410 reflectivity for varying concentrations of H_2O in mantle olivine using data from Wood (1995) to provide phase proportions through the transition interval. Compared to anhydrous mantle, the 0.2–0.5 Hz rms reflection coefficient is halved if 600 ppm water is present, and is ~1/3 at 1000 ppm concentration. Thus lateral variations in mantle water content can significantly affect 410 reflectivity.

By comparison, temperature effects are smaller. Although Fe–Mg partitioning between α and β depends on temperature (Bina & Wood 1987; Katsura & Ito 1989), the overall effect on reflectivity is weak but frequency-dependent (Bina & Helffrich 1994). Averaging reflectivity between 0.2 and 0.5 Hz yields a change of about ±10 per cent over ±400 °C (Fig. 5). The full 800 °C range approaches or exceeds the largest thermal perturbations anticipated at transition-zone depths, the temperature difference between subducted lithospheric slabs and ambient mantle (Helffrich, Stein & Wood 1989), and excess plume temperatures (Sleep 1992). The maximum plausible thermal effects are equivalent to a 100 ppm change in mantle

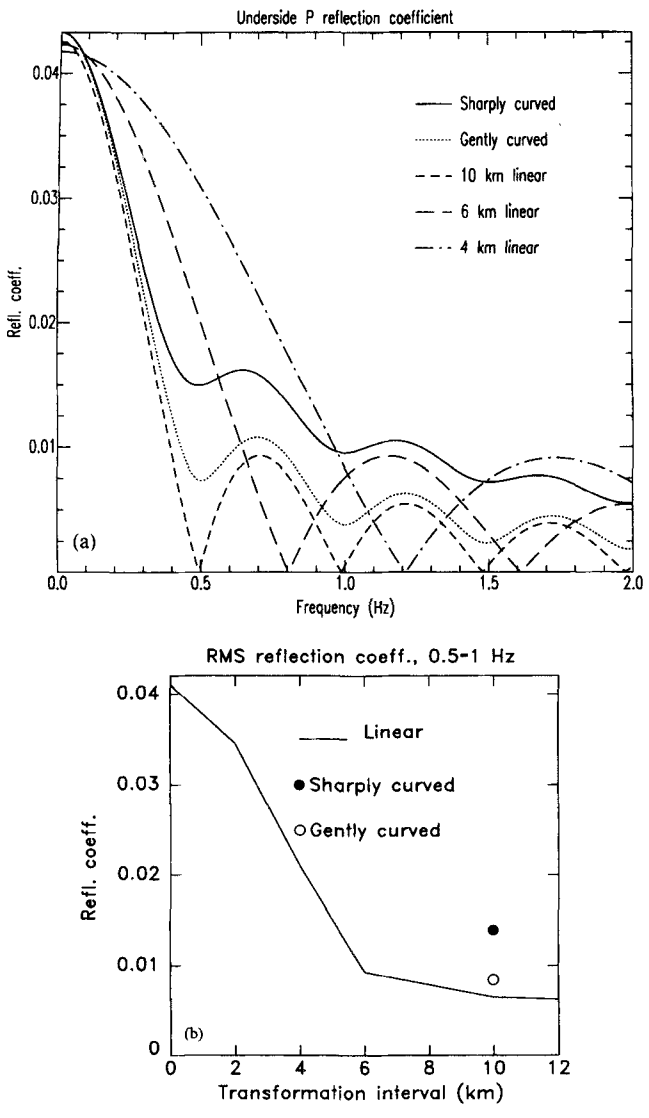

Figure 3. Underside P reflection coefficients for 4, 6 and 10 km linear gradients and for the schematic profiles in Fig. 2, simulating $P'_{410}P'$ reflectivity at 72°(18° vertical incidence angle) (Benz & Vidale 1993). (a) Frequency-dependent reflection coefficients, showing the slower decay of high-frequency reflected energy from realistic transformation profiles compared to linear ones. (b) Dependence of the rms reflection coefficient between 0.5 and 1 Hz on transformation interval thickness. The sharply curved phase boundaries, with a 10 km transition interval, yield reflectivity equivalent to a ~5 km linear gradient. The more gently curved phase boundaries lead to reflectivities equivalent to 7 km, thinner than the full 10 km transition interval in each case.

olivine H_2O content, underscoring the stronger sensitivity to chemical rather than to temperature differences.

4 DISCUSSION

In the 0.5 to 1 Hz band, the underside P reflectivities of the thinner profiles (Fig. 4) are comparable to those of a linear 4 km gradient against which the observations of Benz & Vidale (1993) of underside reflections of $P'P'$ from the 410 km discontinuity were compared. Notwithstanding their claims to the contrary, as well as those of others (Yamazaki & Hirahara 1994), these observations are quite compatible with olivine

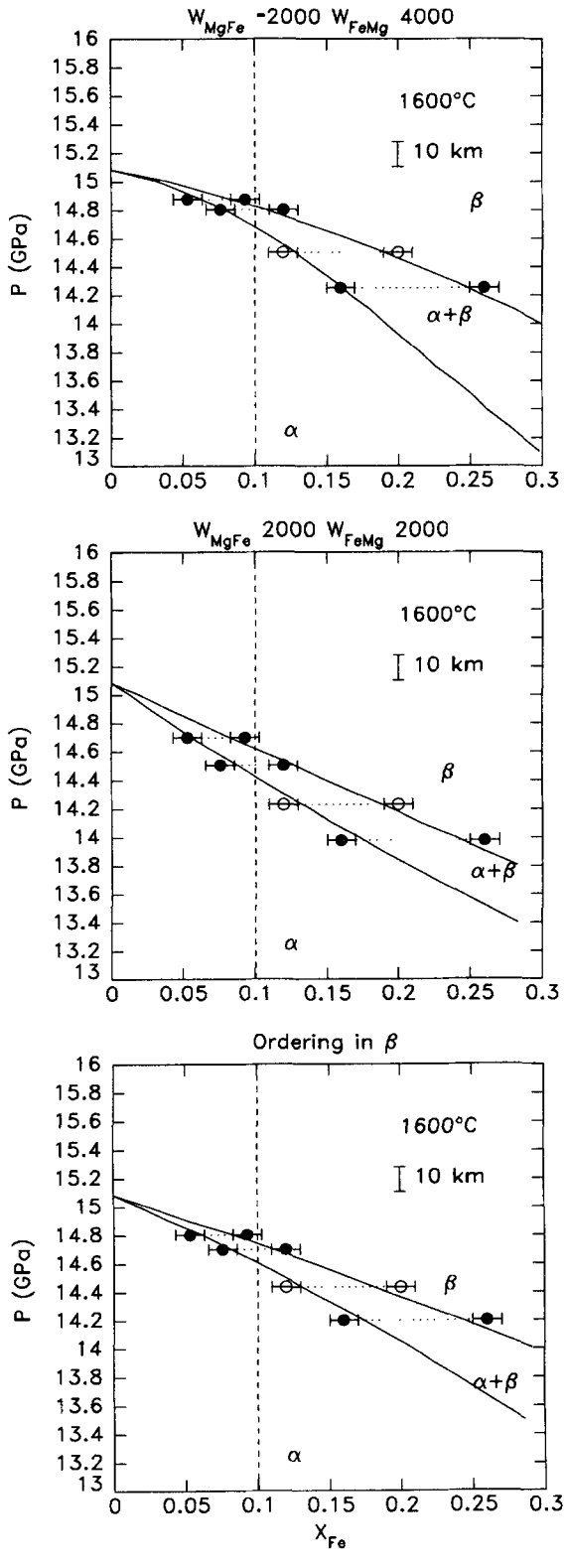

Figure 4. Calculated phase diagrams compatible with (Fe,Mg) partitioning at 1600 °C. The experimentally determined coexisting α and β Fe contents (Katsura & Ito 1989) are linked with dotted tie-lines, with open symbols denoting partitioning determined by BJW at the Bayerisches Geoinstitut. Uncertainties are ± 1 mol per cent in composition and ± 1.5 GPa in pressure. Heading each panel are the subregular interaction parameters (W_{MgFe} and W_{FeMg} for mixing on two sites, in cal.) pertaining to each diagram. See Table 1 for ordering model parameters.

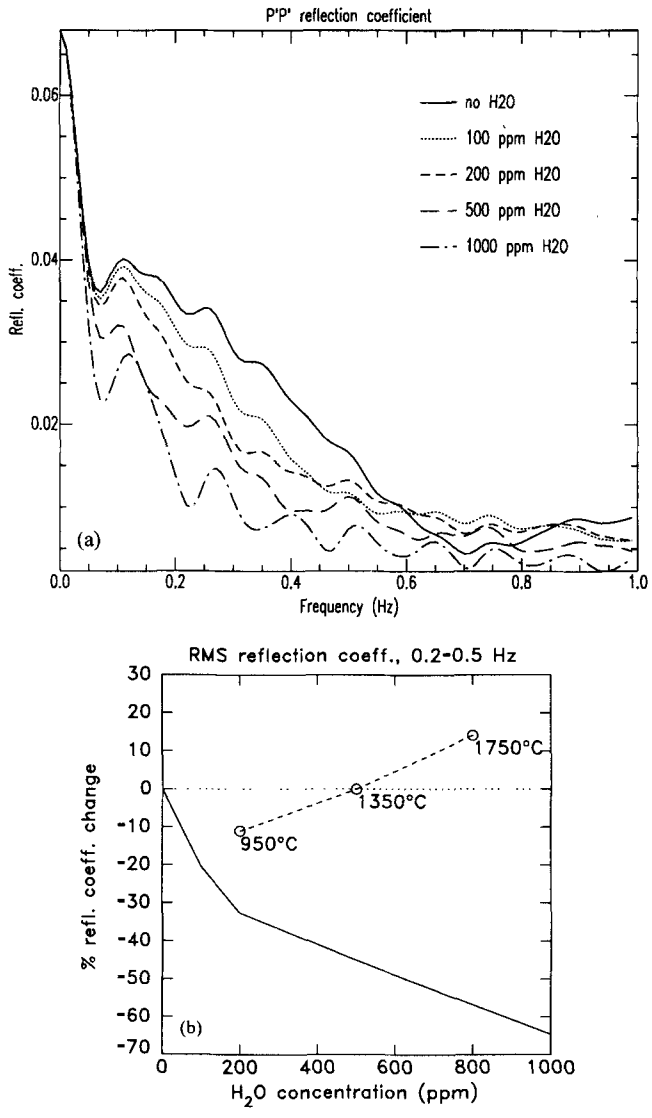

Figure 5. (a) Frequency-dependent reflection coefficients for $P'_{410}P'$ for varying H_2O concentrations. (b) Dependence of 0.2–0.5 Hz rms reflection coefficients on H_2O concentration (solid line) and temperature changes (dashed line). The reflection coefficient change relative to 'normal' conditions is shown in each case: anhydrous conditions and along a 1350 °C adiabat (Bina & Helffrich 1994). A 400 °C change in temperature yields a 10 per cent reflectivity change, equivalent to the effect of 50 ppm H_2O added to anyhdrous mantle. Thus discontinuity reflectivity is much more sensitive to H_2O concentration than temperature.

$\alpha \rightarrow \beta$-modified-spinel phase-transition intervals up to 10 km thick (Fig. 3b), as also shown by Neele (1996). Our results indicate that even 4 km thick transition profiles are feasible given the available (Fe,Mg) partitioning data between α and β phases (Fig. 4). Thus, the phase-transition model for the 410 km discontinuity may not be ruled out simply on the basis of transition thickness.

Of additional interest is the apparent variability in 410 km discontinuity thickness estimates, ranging from 4 to 35 km (Sobel 1978; Benz & Vidale 1993; Priestley *et al.* 1994; Yamazaki & Hirahara 1994; Vidale *et al.* 1995; Neele 1996). Bina & Helffrich (1994) attributed this variability to temperature differences in the mantle. Fig. 5 indicates a significantly greater sensitivity to H_2O concentration between 0.2 and 0.5 Hz. Regionally, the H_2O contents of MORB glasses, derived by melting of the mantle, vary by a factor of 4 (Michael 1994). Thus lateral variations in H_2O or other minor constituents such as Mn and Ni, which in general also broaden the transition interval (Wood 1995), may be a major source of reflectivity variation. The fact that the 410 km discontinuity is visible at all at short periods suggests that it provides a useful constraint on bulk-mantle water content.

While H_2O significantly affects 410 reflectivity, it does not significantly change the apparent depth. This is in contrast to the effect of increasing temperature, which both narrows and deepens the discontinuity. If the principal reason for variability in transformation width is lateral temperature variation, then substantial '410' depth variations should be seen because the P–T slope of the α–β transformation is large (Bina & Helffrich 1994). The 410 is, however, less variable in depth as well as less frequently seen than the 660. These characteristics are more compatible with a response to variations in mantle H_2O content, which affects reflectivity (Fig. 5a) but not the apparent depth of the discontinuity.

ACKNOWLEDGMENTS

We thank D. Rubie and H. Paulssen for thoughtful reviews and John Vidale for 410 reflectivity information and for comments on an earlier version of the manuscript.

REFERENCES

Akaogi, M., Ito, E. & Navrotsky, A., 1989. Olivine-modified spinel–spinel transitions in the system Mg_2SiO_4–Fe_2SiO_4: Calorimetric measurements, thermochemical calculation, and geophysical application, *J. geophys. Res.*, **94,** 15 671–15 685.

Aki, K. & Richards, P.G., 1980. *Quantitative Seismology*, Vol. 1, Freeman, New York, NY.

Benz, H. & Vidale, J., 1993. Sharpness of upper-mantle discontinuities determined from high-frequency reflections, *Nature,* **365,** 147–150.

Bernal, J.D., 1936. Commentary, *Observatory,* **59,** 268.

Bina, C.R. & Helffrich, G., 1994. Phase transition Clapeyron slopes and transition zone seismic discontinuity topography, *J. geophys. Res.*, **99,** 15 853–15 860.

Bina, C.R. & Wood, B.J., 1987. The olivine–spinel transitions: Experimental and thermodynamic constraints and implications for the nature of the 400 km seismic discontinuity, *J. geophys. Res.*, **92,** 4853–4866.

Helffrich, G.R., Stein, S. & Wood, B.J., 1989. Subduction zone thermal structure and mineralogy and their relationship to seismic wave reflections and conversions at the slab/mantle interface, *J. geophys. Res.*, **94,** 753–763.

Jeanloz, R. & Thompson, A., 1983. Phase transitions and mantle discontinuities, *Rev. Geophys. Space Phys.*, **21,** 51–74.

Katsura, T. & Ito, E., 1989. The system Mg_2SiO_4–Fe_2SiO_4 at high pressures and temperatures: Precise determination of stabilities of olivine, modified spinel and spinel, *J. geophys. Res.*, **94,** 15 663–15 670.

Kennett, B.L.N. & Engdahl, E.R., 1991. Traveltimes for global earthquake location and phase identification, *Geophys. J. Int.*, **105,** 429–465.

Lees, A.C., Bukowinski, M.S.T. & Jeanloz, R., 1983. Reflection properties of phase transition and compositional change models of the 670-km discontinuity, *J. geophys. Res.*, **88,** 8145–8159.

Meijering, J.L. & Rooymans, C.J.M., 1958. On the olivine–spinel transition in the Earth's mantle, *Proc. Konin. Ned. Akad. van Wetensch., B,* **61,** 333–344.

Michael, P., 1994. Evidence from trace elements and H_2O for regionally distinctive sources of depleted MORB: Implications for evolution of the depleted mantle, *Mineral Mag.*, **58A,** 607–608.

Neele, F., 1996. Sharp 400-km discontinuity from short-period P reflections, *Geophys. Res. Lett.*, **23,** 419–422.

Priestley, K., Cipar, J., Egorkin, A. & Pavlenkova, N., 1994. Upper-mantle velocity structure beneath the Siberian platform, *Geophys. J. Int.*, **118,** 369–378.

Revenaugh, J. & Jordan, T.H., 1991. Mantle layering from ScS reverberations, 2. The transition zone, *J. geophys. Res.*, **96,** 19 763–19 780.

Richards, P.G., 1972. Seismic waves reflected from velocity gradient anomalies within the Earth's upper mantle, *Z. Geophys.*, **38,** 517–527.

Ringwood, A.E., 1969. Phase transformations in the mantle, *Earth planet. Sci. Lett.*, **5,** 401–412.

Sawamoto, H. & Horiuchi, H., 1990. β $(Mg_{0.9},Fe_{0.1})_2SiO_4$: Single crystal structure, cation distribution and properties of coordination polyhedra, *Phys. Chem. Miner.*, **17,** 293–300.

Sleep, N.H., 1992. Hotspot volcanism and mantle plumes, *Ann. Rev. Earth planet. Sci.*, **20,** 19–43.

Sobel, P., 1978. The phase P'DP' as a means for determining upper mantle structure, *PhD thesis,* University of Minnesota.

Thompson, J.B., 1967. Thermodynamic properties of simple solution, in *Research in Geochem.*, Vol. 11, pp. 340–361, ed. Abelson, P.H., Wiley, New York, NY.

Vidale, J.E., Ding, X.-Y. & Grand, S.P., 1995. The 410-km-depth discontinuity: A sharpness estimate from near-critical reflections, *Geophys. Res. Lett.*, **22,** 2557–2560.

Wiser, N.M. & Wood, B.J., 1991. Experimental determination of activities in Fe-Mg olivine at 1400K, *Contrib. Mineral. Petrol.*, **108,** 146–153.

Wood, B., 1995. The effect of H_2O on the 410-kilometer seismic discontinuity, *Science,* **268,** 74–76.

Yamazaki, A. & Hirahara, K., 1994. The thickness of upper mantle discontinuties, as inferred from short-period J-Array data, *Geophys. Res. Lett.*, **21,** 1811–1814.